Article:
Johnson, L.D.V, Aleemardani, M. orcid.org/0000-0001-8261-4046, Atkins, S. orcid.org/0000-0003-3806-0968 et al. (2 more authors) (2024) Emulsion templated composites: porous nerve guidance conduits for peripheral nerve regeneration. Materials & Design, 239. 112779. ISSN 0264-1275

https://doi.org/10.1016/j.matdes.2024.112779

Materials & Design 239 (2024) 112779

Contents lists available at ScienceDirect

Materials & Design

journal homepage: www.elsevier.com/locate/matdes

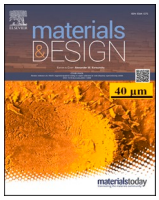

Emulsion templated composites: Porous nerve guidance conduits for peripheral nerve regeneration

Louis D. V. Johnson [a,c], Mina Aleemardani [a], Simon Atkins [b,c], Fiona M. Boissonade [b,c], Frederik Claeyssens [a,c,*]

[a] Kroto Research Institute, Department of Materials Science and Engineering, University of Sheffield, Broad Lane, Sheffield S3 7HQ, UK
[b] School of Clinical Dentistry, University of Sheffield, Claremont Crescent, Sheffield S10 2TN, UK
[c] The Neuroscience Institute, University of Sheffield, Sheffield, UK

ARTICLE INFO

Keywords:
Nerve guidance conduit
Porous
Composite

ABSTRACT

Peripheral nerve regeneration fails following more severe injuries where the gap between nerve stumps is too large. Nerve guidance conduits (NGCs) can be implanted to connect the nerve stumps and provide a regenerative microenvironment. This study shows that poly(glycerol sebacate)-methacrylate (PGS-M), a photocurable and biodegradable elastomer, can be used to fabricate porous NGCs. Further, novel developments in emulsion templating techniques are used to generate composite structures and their mechanical properties are investigated. The most appropriate composite for nerve tissue repair had a compressive and tensile Young's modulus of 0.168 MPa and 0.694 MPa respectively, much closer to that of native nerve tissue than previously used polymers. SEM images revealed high porosity/interconnectivity of NGCs, important for the diffusion of nutrients to further aid nerve regeneration. FITC-Dextran (150 kDa) effectively diffused through conduit walls. Histological analysis demonstrated the small pore size successfully prevented infiltration of fibroblasts. *In vitro* studies indicated that the NGCs were cytocompatible. E*x vivo* analysis showed that neurons of embryonic chick dorsal root ganglia grew on the surface of the conduits, and Schwann cells migrated effectively along the lumen. This study demonstrates a novel way of fabricating porous scaffolds and demonstrates their potential for the treatment of PNI.

1. Introduction

The peripheral nervous system (PNS) is the network of nerves that extend away from the spinal cord to innervate surrounding tissues and extremities. Peripheral nerve injuries (PNI) are more common than spinal cord injuries, affecting over 300,000 Europeans annually [1]. Unlike the central nervous system, the PNS has an innate capacity for self-repair due to the presence of Schwann cells that assist in the regeneration of damaged axons. However, in more severe injuries where the nerve may be completely severed, natural healing is unlikely and surgical intervention is required. Anastomosis (direct end-to-end suture of nerve stumps) has success rates as high as 70 % in restoring nerve function [2] but is limited to very small gap injuries as excessive stretching of the nerve can cause further damage [3]. The current gold standard for larger nerve gap injuries is the nerve autograft, a segment of nerve from the donor's own body. This natural scaffold contains autologous Schwann cells that secrete neurotrophic factors and extracellular matrices to guide regenerating axons. However, there are disadvantages to this treatment including donor site morbidity, a limited supply of autologous donor nerve, and the general risks involved with a second site of surgery [4].

An alternative to the autograft is the nerve guidance conduit (NGC); a tubular device that encloses the space between proximal and distal nerve stumps providing a regenerative microenvironment for axonal regeneration. These scaffolds can be made from natural or synthetic materials. Those that are made from natural materials such as collagen display cell adhesion molecules which act as topographical cues for regrowing axons and Schwann cells [5]. Unfortunately, natural materials also have high batch-to-batch variability and often inappropriate mechanical properties for nerve repair [6]. Synthetic polymers could be considered advantageous in that they are more reproducible and have tuneable mechanical properties. However, commercially available NGCs

Abbreviations: PNI, Peripheral nerve injury; NGC, nerve guidance conduit; PGS, poly(glycerol sebacate; PGS-M, poly(glycerol sebacate)-methacrylate; PNS, peripheral nervous system.

* Corresponding author at: Kroto Research Institute, Department of Materials Science and Engineering, University of Sheffield, Broad Lane, Sheffield S3 7HQ, UK.
E-mail address: f.claeyssens@sheffield.ac.uk (F. Claeyssens).

https://doi.org/10.1016/j.matdes.2024.112779
Received 6 December 2023; Received in revised form 26 January 2024; Accepted 18 February 2024
Available online 22 February 2024

made from synthetic polymers such as poly-DL-lactide-caprolactone (PDLLA/CL) and polyglycolic acid (PGA) present two main problems. Firstly, they are far stiffer than the native tissue which can cause compressive damage to the surrounding tissue [7] and be impractical due to an inability to bend with natural movements of the body. Secondly, NGCs are yet to prove as or more effective than the nerve autograft [8]. This is likely due to the fact they are of simple design, lacking the factors of the autograft that contribute towards successful regeneration. Thus, a NGC that is i) made from a more suitable material and ii) has a better design so that nerve regeneration is more successful is desirable.

Poly(glycerol sebacate) (PGS) is a biodegradable material that has gained recent attention in tissue engineering having been investigated as a biomaterial, particularly for soft tissues such as cardiac patches [9,10], tympanic perforations [11] and retinal repair [12]. Synthesised via a two-step polycondensation reaction between glycerol and sebacic acid, PGS is an inexpensive polymer with a versatile structure due to an available hydroxyl group for functionalisation. Methacrylation of these hydroxyl groups results in the synthesis of poly(glycerol sebacate)-methacrylate (PGS-M) and enables photocrosslinking and tunability of mechanical properties [13,14]. Yet, there is currently just one study that has assessed PGS-M as a 3D structure for peripheral nerve repair. Singh *et al.* [15] demonstrated the favourable mechanical properties, 3D-printability, and capacity for nerve regeneration of PGS-M NGCs *in vivo*. Nonetheless, the conduits in the work of Sing *et al.* [15] were still simple tubes of solid PGS-M, which warrants further investigation into PGS-M conduits with an improved design.

The diffusion of nutrients and waste products through a NGC is advantageous for nerve regeneration [16]. While nonporous conduits permit small amounts of nutrient diffusion at either end, this is likely to be insufficient for large nerve gap injuries. Porosity within NGC walls offers a solution to this problem, allowing nutrient diffusion across the entire length of the conduit. However, considerations to pore size must be made as conduits with large pores (>10 μm diameter) allow the infiltration of scar tissue-secreting fibroblasts, inhibitory to nerve regeneration [16–19]. Therefore, it is likely that a semi-permeable conduit with small pores (<10 μm diameter) will prove more effective.

Emulsion templating techniques have been previously utilised to create highly interconnected porous structures with a small pore size [20]. Some polymers can form a water-in-oil emulsion where the continuous polymer phase can be crosslinked and then dehydrated to generate a porous structure. Polymerised high internal phase emulsions (polyHIPEs) are a specific example of this technique, where the dispersed phase (water) exceeds 74 % of the total emulsion volume resulting in small, highly interconnected pores [21,22]. However, polyHIPE structures are often mechanically weak, even if fabricated from stiffer polymers, due to air comprising the majority of the structure. The aim of this study is to fabricate porous NGCs with more favourable mechanical properties by developing existing emulsion templating methods before assessing their efficacy *in vitro* and *ex vivo* for the treatment of PNI. This is obtained via a previously unreported method for making a polymer-polyHIPE composite, via simple mixing in the base polymer (PGS-M) into the HIPE. This results in dispersion of polymer droplets in the HIPE to obtain a composite structure. This allowed us to tune the mechanical structure of the porous constructs without greatly disrupting the interconnected porous nature of the resulting polyHIPE.

2. Materials and methods

2.1. Materials

NG108-15 cells, sebacic acid, glycerol, Dulbecco's modified Eagle's medium (DMEM), foetal bovine serum (FBS), penicillin/streptomycin (PS), l-glutamine, amphotericin B, forskolin, resazurin, trypsin, formaldehyde, diphenyl(2,4,6-trimethylbenzoyl) phosphine oxide/2-hydroxy-2-methylpropiophenone (photoinitiator), methacrylic anhydride, triethylamine, mono methyl ether of hydroquinone (MEHQ), dichloromethane (DCM), ethanol and FITC-dextran (150 kDa) were all purchased from Sigma Aldrich, UK. DPX was purchased from Merck, UK. Hypermer was purchased from Croda. L929 cells, CellTrace™ Calcein Green, AM (20 × 50 μg), ethidium bromide (10 mg ml^{-1}), mouse anti-beta-III-tubulin antibody, rabbit anti-mouse IgG antibody conjugated to Alexa Fluor 488 and goat anti-rabbit IgG (H + L, cross-adsorbed) antibody conjugated to Alexa Fluor 488 were purchased from ThermoFisher Scientific, UK. Horse anti-mouse IgG (H + L) antibody conjugated to Texas Red was purchased from Vector Laboratories. Recombinant anti-S100 beta antibody [EP1576Y] was purchased from Abcam. 9–0 polyamide sutures were purchased from Ethicon and 6–0 polypropylene sutures were purchased from Lux Sutures.

2.2. Synthesis of PGS prepolymer

The synthesis of PGS has been previously described in the literature [23]. Briefly, a polycondensation reaction between sebacic acid and glycerol at a 1:1 M ratio was performed at 120 °C for 24 h under nitrogen flow. Then, the reaction was performed for a further 24 h under vacuum conditions before collection of the PGS prepolymer. The prepolymer was analysed with NMR and GPC.

2.3. Functionalisation of PGS prepolymer into PGS-M

The PGS prepolymer was cooled in an ice bath and then dissolved in DCM. MEHQ was added to inhibit spontaneous photopolymerisation. PGS contains 195 mmol of hydroxyl groups per 50 g of polymer. Methacrylic anhydride and triethylamine (0.8 mol/mol of hydroxyl groups on PGS) were added dropwise to allow the methacrylation of 80 % of the available hydroxyl groups on the PGS prepolymer. The flask was covered in foil and the reaction was performed for 24 h at room temperature. For purification, the polymer was washed 3 times in 30 mM hydrochloric acid solution. Any remaining solvent was removed from the polymer via rotary evaporation. Samples of PGS-M were analysed via NMR and GPC.

2.4. PolyHIPE and composite scaffolds creation

Polymerised high internal phase emulsions (polyHIPEs) with an estimated porosity of 76.19 % were created by mixing 0.5 g PGS-M with 0.05 g Hypermer and melted using a heat gun. 0.5 g toluene was added and mixed for 2 min using a magnetic stirrer at 550 rpm. The glass tube was set up in a water bath set at 37 °C. Water was added at a rate of 1 drop every 2 s until a total of 4 ml of water was added. 0.2 g of photoinitiator was added at the end and the emulsion was covered with foil and left to mix for 3 min. The emulsion was injected into various moulds (described later) prior to photocrosslinking. To fabricate composite PGS-M scaffolds, 0.5, 1.0 or 2.0 g of PGS-M was added to the HIPE and mixed at 200 rpm. These mixtures of HIPE and PGS-M were stirred for 15 min prior to photocrosslinking. Samples were prepared for imaging via scanning electron microscopy (SEM) by freeze-drying for 24 h and then sectioning by using a scalpel blade. In total, four types of scaffold were created: polyHIPE scaffold (HIPE) and then three composites (HIPE + 0.5G, HIPE + 1G and HIPE + 2G). For all experiments other than SEM, compression and uniaxial tensile testing, the HIPE + 1G composite was used.

2.4.1. Compression test

Emulsions were injected into cylindrical polydimethylsiloxane (PDMS) moulds and cured with UV light emitted from a mercury lamp (100 W, Omnicure S1000) for 5 min, flipped over, and cured for a further 5 min. A MultiTest-dV tester (Mecmesin, Slinfold, UK) was used with a load cell of 25 N. Compression testing of the samples was conducted with a load cell of 25 N, set at 1 N/s with a maximum load of 25

N. The Young's modulus was calculated using the linear (elastic) region of the stress–strain curves of each sample.

2.4.2. Uniaxial tensile test

Emulsions were injected into dog-bone shaped PDMS moulds and cured with UV light emitted from a mercury lamp (100 W, Omnicure S1000) for 5 min, flipped, and cured for a further 5 min. A MultiTest-dV tester (Mecmesin, Slinfold, UK) was used with a load cell of 25 N, a grasp distance of 10 mm and extension rate of 1 mm/s. Force and max elongation were recorded, and the Young's modulus was calculated.

2.5. Porosity quantification using helium pycnometry

3 samples for each material were made using silicon cylindrical moulds with an estimated height of 3.4 mm and diameter of 9.5 mm. These samples were washed using methanol and ethanol for an hour each, prior to 3 PBS washes. The samples were freeze-dried for 24 h and their dimensions were measured using digital callipers to calculate the macroscopic volume. The samples were examined using helium pycnometry (AccuPyc 1340, Micromeritics, USA). For one reading, all 3 samples were loaded into a 0.1 cm^3 chamber insert and the chamber was pressurised at 19 psi. The true volume of the samples (the volume of the solid component of the samples) was determined based on the amount of helium added to the chamber. The porosity of each samples was calculated using Equation (1). A bulk PGS-M sample was used as a control. The density for bulk PGS-M was given by the pycnometer (1.18 g / cm^3) and this was used to estimate the porosity for each sample using Equation (2). 12 pores were randomly measured using ImageJ from 3 SEM images of each sample (36 pores in total) to calculate the mean pore diameter.

$$\left(1-\frac{truevolume}{macroscopicvolume}\right)\times 100 = porosity(\%) \tag{1}$$

$$100-\left(\frac{volumeofoilphase}{totalvolumeofemulsion}\times 100\right) = estimatedporosity(\%) \tag{2}$$

2.6. NGC fabrication

The emulsion was drawn up into a 1 ml syringe and injected into a handcrafted mould that had a diameter of 2 mm, with a needle of 1.1 mm diameter running through the length of the mould. Samples were cured via UV radiation for 5 min on each side, for a total of 10 min, and were removed from the moulds and trimmed down to a length of 5 mm using a scalpel.

For SEM preparation, NGCs were freeze dried for 24 h prior to the sectioning of conduits using a scalpel for internal and external visualisation of the conduits. The samples were gold-coated and imaged using a scanning electron microscope (Inspect F, FEI) where the accelerating voltage and the spot size were 5 kV and 3, respectively.

2.7. PGS-M flat disc creation

Flat nonporous or porous PGS-M discs were created. For the nonporous discs, photoinitiator (diphenyl(2,4,6-trimethylbenzoyl) phosphine oxide/2-hydroxy-2-methylpropiophenone) was added to PGS-M before UV-curing in a flat sheet of 1 mm depth. This was achieved by compressing the polymer between two glass slides. Flat discs were then punched out using a biopsy punch with the same dimensions of a 24 well plate. For the porous discs, the emulsion was injected into a PDMS mould with the same dimensions of the well of a 24 well plate, UV-cured, and then sliced into discs (2 mm thickness) using a scalpel.

2.8. PGS-M sample sterilisation

PGS-M scaffolds were washed with > 99.8 % methanol and 70 % ethanol for 1 h each. Then, the scaffolds were washed three times (30 min each wash) with phosphate-buffered saline (PBS).

2.9. Cell culture

NG108-15 cells (passage 16) or L929 cells (passage 12) were restored from liquid nitrogen storage and cultured in Dulbecco's modified Eagle's medium (DMEM), containing 10 % FBS (v/v), 0.25 μg/ml amphotericin B, 100 units/ml penicillin, 100 μg/ml streptomycin and 2 mM L-glutamine and incubated at 37 °C with 5 % CO_2. Cells were passaged upon reaching 80 % by PBS washing then addition of 5 ml trypsin-EDTA solution (Sigma-Aldrich, UK) for 3 min. Cells were counted using a haemocytometer before seeding onto scaffolds.

2.10. Cell metabolic activity

PGS-M porous or nonporous discs were incubated in serum-containing medium for 1 h prior to seeding. NG108-15 cells were seeded at a density of 1×10^5 cells (40 μl droplet) onto the substrates and were initially incubated for 1 h to allow adhesion onto scaffolds. Then, 1 ml of serum-containing medium was added and replaced every 2 days. Tissue culture plastic (TCP) was used as a positive control. The metabolic activity of NG108-15 cells was measured using the resazurin reduction assay. A 1 mM resazurin working stock solution was mixed with cell culture medium in a 1:10 ratio to create a resazurin/medium solution. At days 1, 4 and 7 of the experiment, scaffolds were moved to fresh well plates and 1 ml resazurin media solution was added. After 4 h of incubation, 200 μl of solution for each well was pipetted into a 96 well plate and readings were taken using a spectrofluorometer (FLX800, BIOTEK Instruments, Inc.) which measured excitation and emission wavelengths of 540 nm and 630 nm, respectively.

2.11. Live/dead assay

NGCs were dissected bilaterally, creating hemi-conduits to allow imaging. The hemi-conduits were incubated in serum-containing medium for 1 h prior to seeding. NG108-15 cells were seeded at a density of 1×10^5 cells (20 μl droplet) onto hemi-conduits and incubated for 1 h. Then, 1 ml of cell culture medium was added (DMEM containing 10 % FBS (v/v), 0.25 μg/mL amphotericin B, 100 units/ml penicillin, 100 μg/ml streptomycin and 2 mM L-glutamine) and replaced every 2 days. Cells were cultured for either 4 or 7 days prior to the live/dead assay. Calcein green AM and ethidium bromide were diluted in PBS (2 μl ml^{-1} in DMSO, 0.2 μl ml^{-1} in PBS, respectively), added to the samples and incubated for 30 min. The cells were then imaged using a ZEISS LSM880 Airyscan confocal microscope using a 10 × objective for live and dead cells. *Z*-stack images were taken for each sample and projected to a single image.

2.12. Neurite length analysis

NG108-15 cells were seeded onto PGS-M hemi-conduits as reported above. Cells were cultured in serum-containing medium for 48 h to allow adherence and proliferation. After 48 h, the medium was removed and serum-free medium was added (DMEM containing 0.25 μg/ml amphotericin B, 100 units/ml penicillin, 100 μg/ml streptomycin and 2 mM L-glutamine) to induce neuronal differentiation. Cells were either cultured for 4 or 7 days prior to immunocytochemistry assay. Scaffolds were washed with PBS and fixed with 3.7 % formaldehyde solution, then repeatedly washed with PBS between each step. Cells were permeabilised with 0.1 % Triton-X 100 in PBS and blocked with 3 % bovine serum albumin (BSA) in PBS for 30 min each. Primary mouse anti-beta-III-tubulin antibodies (1:1000 titre) were added to the cells (diluted in 1 % BSA solution) and left overnight at 4 °C. Secondary rabbit anti-mouse IgG antibodies conjugated to Alexa Fluor 488 (1:500 titre, diluted in 1 % BSA solution) with DAPI solution (1 μg/ml) were added and left for 3 h

at room temperature. The samples were imaged using an upright ZEISS LSM 510 confocal microscope with a water-dipping 10 × objective (Objective W N-Achroplan 10×/N.A. 0.3, ZEISS, US). *Z*-stack images were taken for each sample and projected to a single image. ImageJ was used for neurite length measurements.

2.13. Embryonic chick dorsal root ganglia explants

Embryonic chicks were incubated for 10 days then sacrificed and prepared for dissection. The dorsal root ganglia (DRG) were harvested and seeded into either the centre of PGS-M hemi-conduits or onto TCP as positive controls. The DRG were initially incubated for 20 min to allow adherence to scaffolds, and then 20 μl of cell culture medium was added (DMEM containing 10 % FBS (v/v), 0.25 μg/ml amphotericin B, 100 units/ml penicillin, 100 μg/ml streptomycin and 2 mM L-glutamine, 0.01 % forskolin). After 30 min, a further 1 ml of medium was added. 500 μl medium was replaced with fresh medium every 3 days. At 14 days of culture, samples were prepared for immunocytochemistry as described above. Schwann cells were immunolabelled with recombinant anti-S100 beta antibody (1:1000 titre) and then goat anti-rabbit IgG (H + L, cross-adsorbed) antibody conjugated to Alexa Fluor 488 (1:500 titre). Neurites were immunolabelled with mouse anti-beta-III-tubulin antibody (1:1000 titre) and horse anti-mouse IgG (H + L) antibody conjugated to Texas Red (1:500 titre). DAPI solution (1 μg/ml) was also added to the secondary antibody solution and left for 3 h at room temperature. Samples were imaged using a ZEISS LSM880 Airyscan confocal microscope (10 × objective) and *z*-stack images were taken and projected to a single image. To measure Schwann cell migration, composite images were created by tiling the images and then, using ImageJ, the distance of the furthest Schwann cell was measured from the centre of the DRG. The chick DRGs were used in line with the NC3Rs guidelines, it is considered more ethical to use embryonic chicks that are not yet considered living vertebrates under the Animals (Scientific Procedures) Act 1986.

2.14. Fibroblast infiltration assay

L929 fibroblasts were seeded at a density of 1×10^5 cells per ml onto PGS-M conduits in a 12 well plate. Cells culture medium was replaced every 2 days (DMEM containing 0.25 μg/ml amphotericin B, 100 units/ml penicillin, 100 μg/ml streptomycin and 2 mM L-glutamine). After 7 days of culture, samples were washed with PBS and fixed with 3.7 % formaldehyde solution, placed in tissue cassettes and then into the Leica TP 1020 tissue processor (Leica Biosystems, UK) for 18 h. The samples were then embedded in wax, and sectioned (5 μm thickness) onto glass slides using a Leica RM2145 microtome (Leica Biosystems, UK). The slides were stained using haematoxylin for 1.5 min and eosin for 5 min, washed with distilled water, dehydrated via a series of IMS washes and then dunked twice in xylene. Using DPX, the slides were mounted before imaging on an optical microscope (Motic BA210, China).

2.15. Fitc-dextran diffusion assay

NGCs were superglued so they stood upright in a 6 well plate. FITC-conjugated dextran with a molecular weight of 150 kDa was diluted in deionised water (0.8 mg per ml), injected into the lumen of the conduits and imaged using an inverted epifluorescent microscope (Olympus). Then, the well was filled with deionised water up until half way up the height of the conduit, being careful not to fully submerge the conduit. An image was taken immediately after the addition of water, and again after 24 h.

2.16. Statistical analysis

Three biological replicates were performed for all experiments, and each included three technical replicates. The exception to this was the compression and uniaxial tensile testing with just five technical replicates. For the mechanical testing and cell metabolic activity assay (on day 7), groups were compared using one-way Tukey analysis of variance (ANOVA) test with multiple comparisons. Two-way ANOVA with a multiple comparison Tukey's post hoc test was used to compare metabolic rates between different time points for the metabolic activity assay at different time points and for the average/maximum neurite length analysis. Data were plotted as means ± standard deviations (SD). Statistical significance was reported using the New England Journal of Medicine (NEJM) style, where P values < 0.05 are considered significant (*), P values < 0.01 (**) and P values < 0.001 (***).

3. Results

3.1. Characterisation of polyHIPE/polymer composites

Four types of PGS-M structure were subjected to compression and tensile testing. To make the composite structures a PGS-M−based HIPE was first produced and then an amount of PGS-M was added to this HIPE. We added 0.5 g, 1 g or 2 g of PGS-M to 5 ml of HIPE emulsion. The compressive Young's moduli of the HIPE, HIPE + 0.5G, HIPE + 1G and HIPE + 2G structures were 0.078 MPa ± 0.004, 0.138 MPa ± 0.018, 0.168 MPa ± 0.008 and 0.64 MPa ± 0.255, respectively. The tensile Young's moduli of the same structures were 0.094 MPa ± 0.018, 0.28 MPa ± 0.112, 0.694 MPa ± 0.198 and 1.772 MPa ± 0.138. The stress–strain curves and graphical representations of Young's moduli can be seen in Fig. 1.

Scanning electron microscopy (SEM) images were taken of cross sections of these scaffolds at 1000 × and 2500 × magnification (Fig. 1E). The images indicate the homogeneity of the porous structure decreased with the increasing amount of polymer added. In the HIPE + 0.5G structure, small chunks of polymer are observed dispersed within the porous structure as a result of mixing the polymer within the emulsion prior to curing. The chunks of polymer appear larger in the HIPE + 1G structure, and larger still in the HIPE + 2G structure to the point where the porosity and interconnectivity is mostly compromised. The porosity of the scaffolds was quantified using helium pycnometry. The porosity and mean pore sizes of each scaffold are summarised in Table 1. The HIPE + 1G structure was selected as the most promising composite for nerve regeneration due to its balance of mechanical properties while maintaining good porosity and interconnectivity. Hence, this composite was used for NGC production and *in vitro* testing.

3.2. Manufacture and suitability of porous PGS-M NGCs

NGCs were successfully manufactured following the protocol explained in the methods section (Fig. 2). The conduits were fabricated from the HIPE + 1G emulsion and, due to the composite structure, better resisted the compressive forces when squeezed between finger and thumb. In addition, these conduits did easily bend up to approximately 45° without much apparent kinking (Fig. 2C) but would immediately regain their original shape once released.

As an initial assessment of *in vivo* suitability, a 5-mm composite conduit was surgically implanted (Fig. 2D) into a culled thy-1-YFP-H mouse (n = 1). The animal was killed using a Schedule-1 killing method, in accordance with the Animals (Scientific Procedures) Act 1986. The left sciatic nerve was exposed and freed from the surrounding tissue. The nerve was transected and the conduit placed into the gap. 1-mm lengths of the proximal and distal nerve stumps were inserted into the conduit (to create a 3-mm gap) and sutured in place using two 9–0 polyamide sutures at each end of the conduit. The flexible conduits were easy to handle and manipulate into position and although soft, they did not tear when the sutures were fastened tightly (Fig. 2D, E). Once secured, the layers of muscle and skin were sutured using 6–0 polypropylene sutures to establish that the conduit did not collapse during wound closure, and the wound was closed. The conduit maintained its

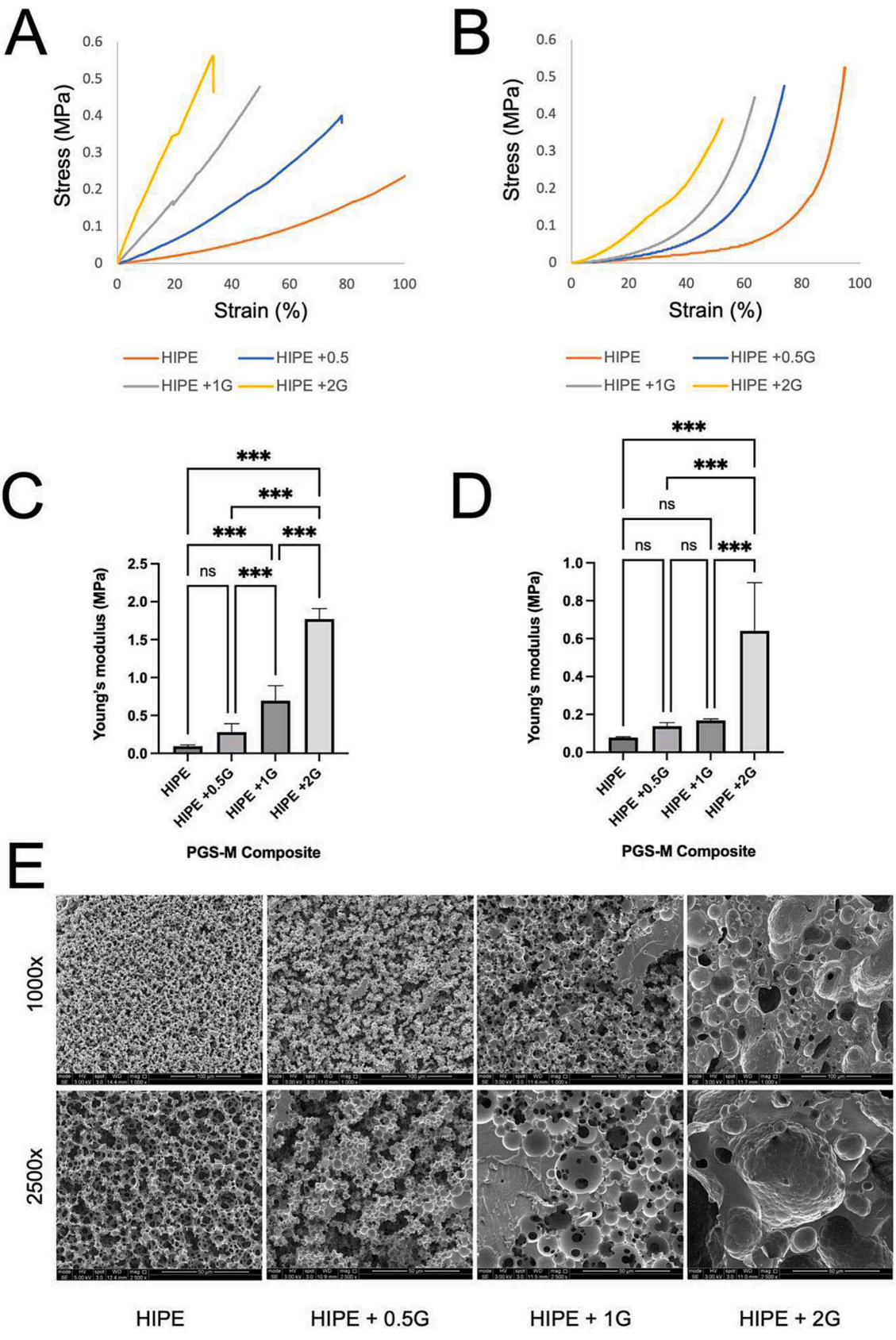

Fig. 1. Characterisation of composite structures fabricated via emulsion templating. A) Uniaxial tensile testing and B) compression testing stress–strain curves of PGS-M composites. C) Tensile Young's modulus of composites. D) Compressive Young's modulus of composites. E) SEM images at 1000× (top row) and 2500× (bottom row) magnification showing how the porous structures are affected by the additional mixing of polymer into the HIPE.

Table 1
Porosity and pore size of various PGS-M scaffolds.

Sample	Estimated porosity (%)	Actual porosity (%)	Mean pore diameter (μm)
HIPE	90.42	86.17	7.28 ± 1.84
HIPE + 0.5G	82.53	74.43	8.13 ± 5.5
HIPE + 1G	75.89	69.85	9.77 ± 7.73
HIPE + 2G	65.37	53.03	29.79 ± 23.89

shape during this process.

3.3. SEM imaging of porous PGS-M NGCs

Fig. 3 shows SEM images of a PGS-M conduit at low (100 × or 128 ×) and high (5000 ×) magnifications. The inner diameter of the conduit was 876 μm. As seen in the previous samples, the homogenous porous structure is interrupted by the dispersion of solid chunks of PGS-M. The pores have a mean diameter of 9.77 ± 7.73 μm and display a high amount of small interconnects between (Fig. 3B). As the emulsion was subjected to shear stress when injected into the moulds before curing, it was important to observe the effects of this on the inner and outer surfaces of the conduit. Fig. 3C shows the effect of this stress on the outer wall of the conduit (cured next to silicone tubing). On this surface, the pores, although collapsed, remained open enough so that the intricate porous structure can be observed in the main bulk of the conduit (Fig. 3D). Fig. 3E shows that the inner wall of the conduit became smooth, having cured while touching the metal needle within the mould. Nonetheless, many small holes can be observed (Fig. 3F) which connect the lumen of the conduits to the porous structure within. As shown by Fig. 3F and 4D, there are small spheroidal artefacts present on the smooth surface of the inner lumen, possibly due to phase inversion of the emulsion prior to curing.

3.4. Cytocompatibility of PGS-M scaffolds

3.4.1. Live/dead assay

NG108-15 cells were cultured on hemi-conduits and stained for live/

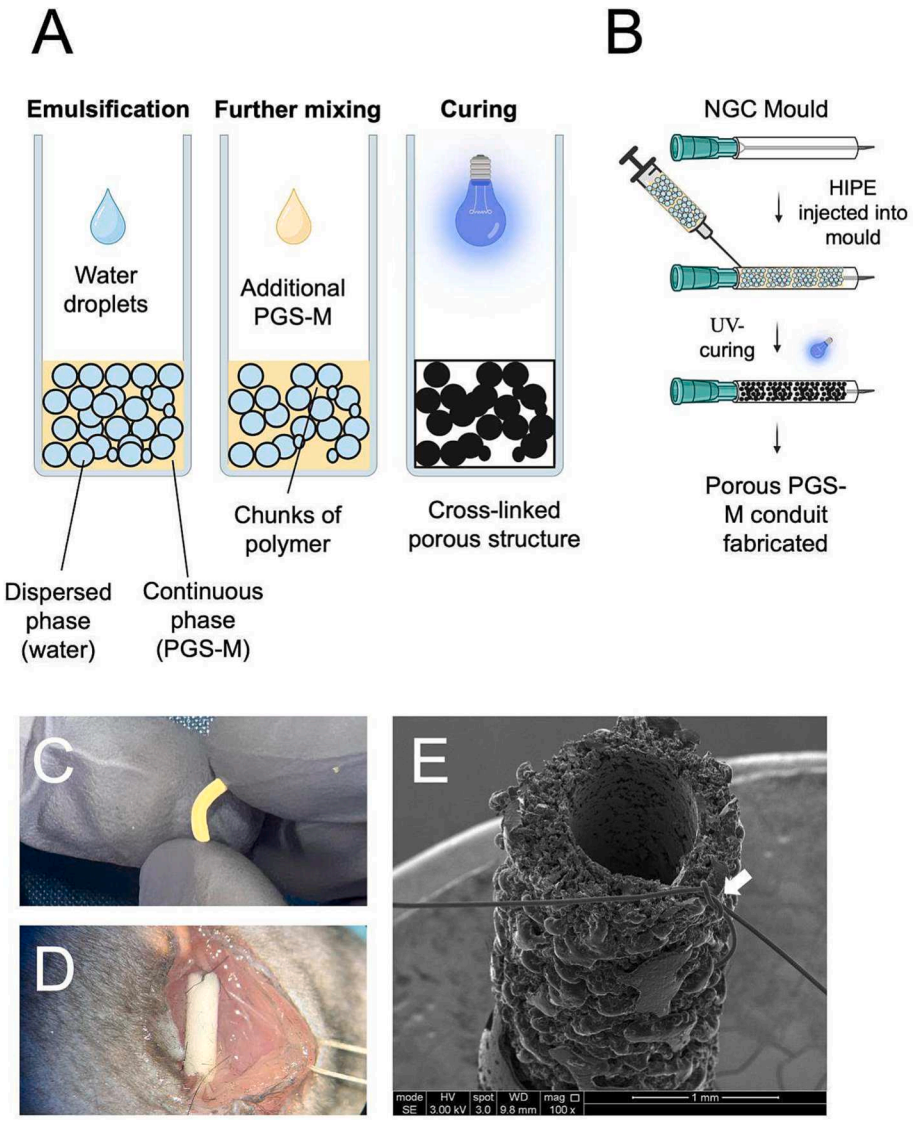

Fig. 2. Manufacture of porous PGS-M NGCs. A) diagram showing PGS-M/water emulsion creation by mixing water droplets (dispersed phase) within PGS-M (continuous phase). The rpm was reduced, and more PGS-M was mixed with the emulsion. UV-curing and removal of water leaves a porous and highly interconnected structure. Schematic created with BioRender.com B) NGCs were created by injecting the emulsion into a mould prior to UV-curing. C) The flexibility of the conduits is shown. D) NGC bridging a 3 mm sciatic nerve gap, sutured in place with polyamide 9–0 sutures, within a mouse. E) Scanning electron microscopy image of a suture tied in place to NGC.

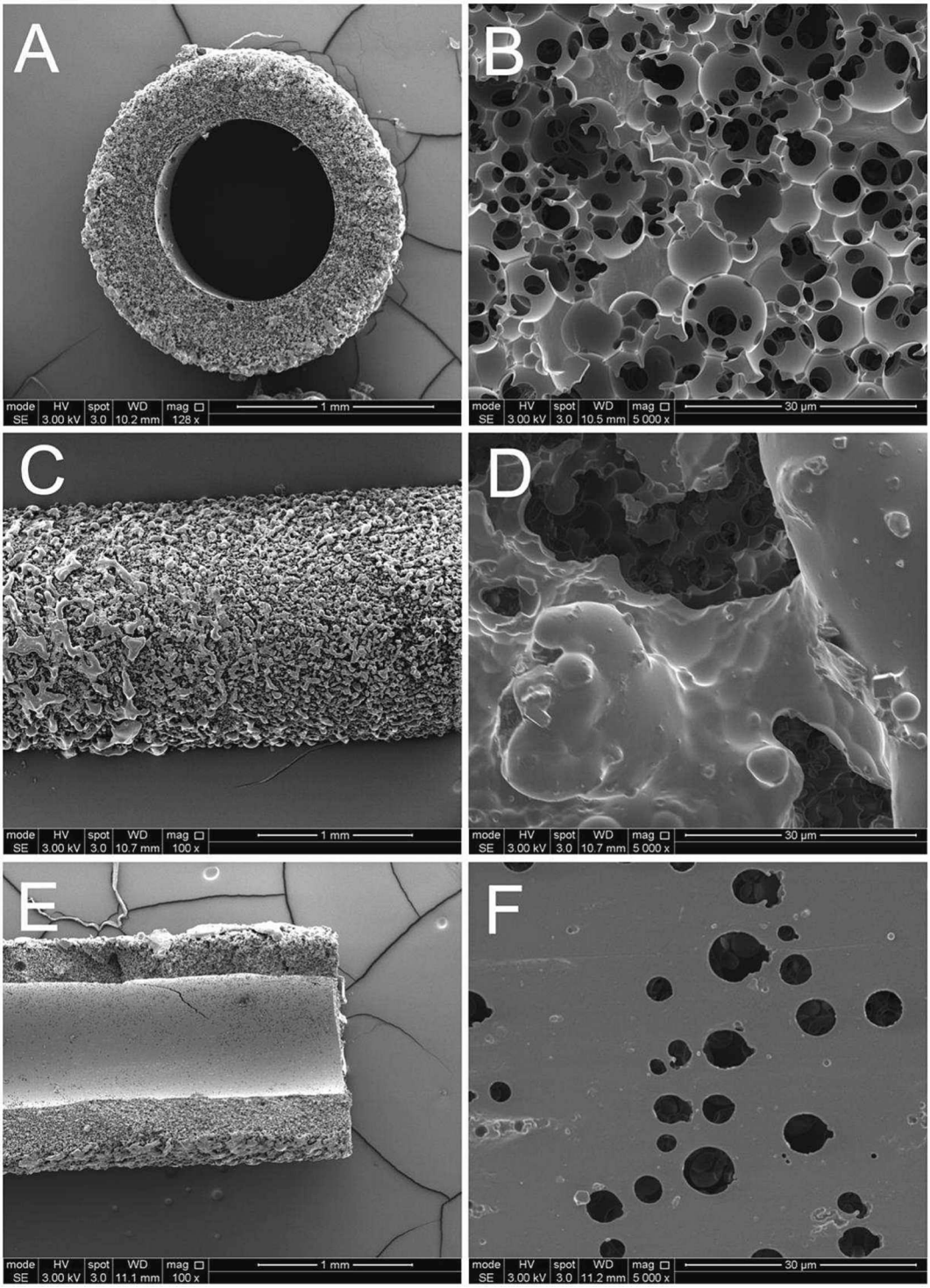

Fig. 3. SEM images of conduits. A) a cross section shown at 128 × and B) at 5000 × magnification. The pores had a mean diameter of 9.77 ± 7.73 µm and were well interconnected. C) the outer conduit wall shown at 100 × and D) at 5000 × magnification. The open porous structure can be seen behind large pieces of nonporous polymer. E) the inner lumen of the conduit shown at 100 × and F) at 5000 × magnification. The wall was smooth due to contact with the mould, yet there were holes in which the porous structure could be seen behind the larger structures on the outer surface.

dead cells with Calcein green AM and ethidium bromide at two time points (4 or 7 days). As negative controls, hemi-conduits with either no cells or dead cells (killed via submersion in 100 % ethanol for 20 min) also underwent live/dead staining (Fig. 4B, C). All images show high levels of background signal from the red channel. This has been shown to be due to autofluorescence of the polymer or to non-specific binding of ethidium bromide to PGS-M, and has been reported previously [24]. Due to this, the spheroidal artefacts identified by SEM imaging (Fig. 3C, 4D) fluoresce brightly red, imitating dead cells (Fig. 4B, C). Consequently, it was not possible to accurately quantify dead cells nor calculate percentage cell viability. Nonetheless, an abundance of living cells can be seen adhered to the bottom of the hemi-conduits after 7 days of culture (Fig. 4A).

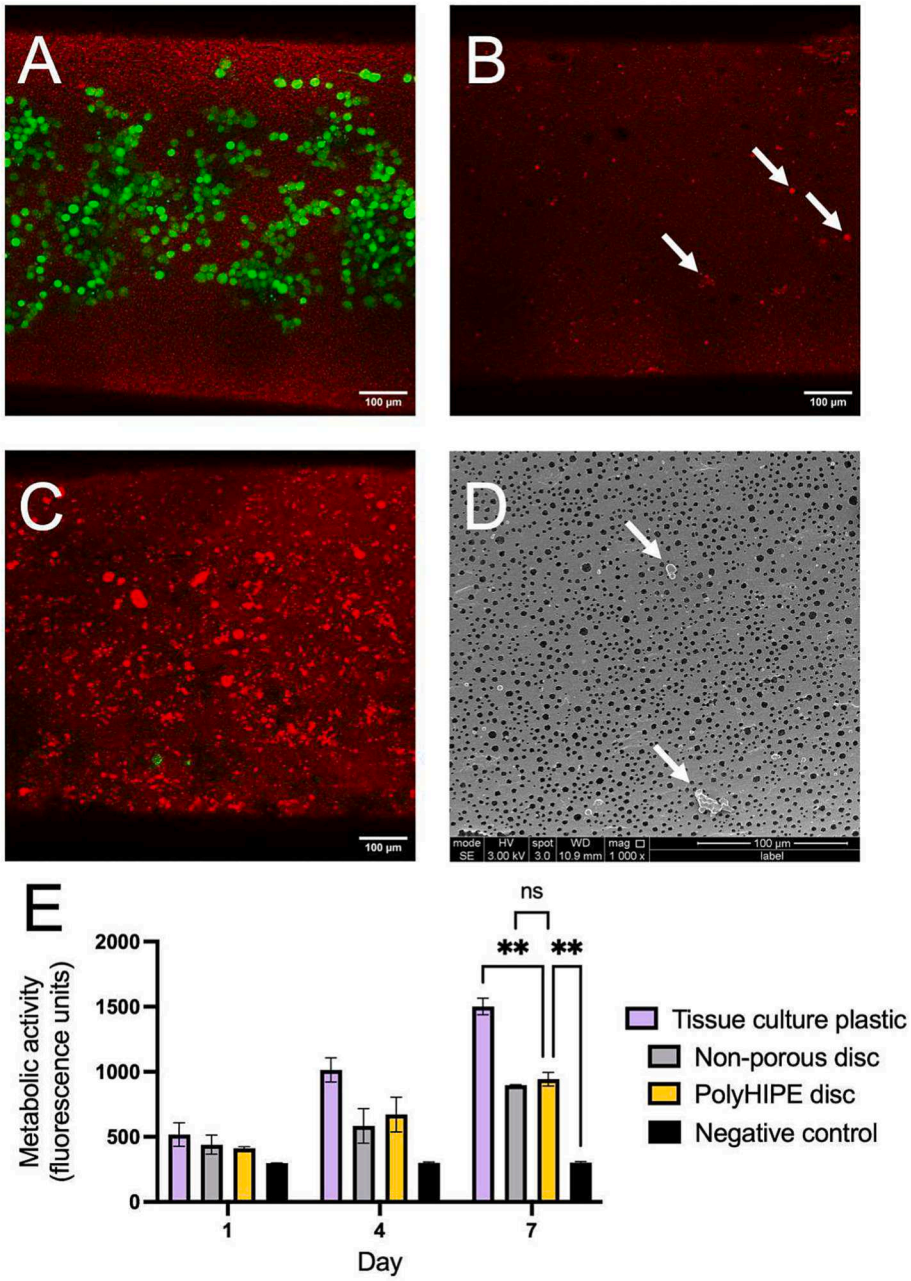

Fig. 4. Cytocompatibility of PGS-M scaffolds. A) Live/dead-stained hemi-conduits after 7 days culture. Live NG108-15 cells were dyed green and dead cells were dyed red. Due to auto-fluorescence and possibly some affinity of ethidium bromide to PGS-M, there was substantial background signal. B) a hemi-conduit after live/dead staining without any cells. The white arrows point to the spheroidal artefacts that brightly fluoresce red, making it difficult to identify and quantify dead cells. C) a hemi-conduit with live/dead staining after submersion in 100 % ethanol for 20 min to show dead cells as negative control. D) SEM image showing the artefacts that fluoresce red after staining. E) metabolic activity of NG108-15 cells after culture on PGS-M discs (** $p < 0.01$; ns = not significant).

3.4.2. Resazurin reduction assay

NG108-15 cells were cultured on porous and nonporous PGS-M discs. The resazurin reduction assay showed that cells metabolic rates increased over a 7-day period on both substrates indicative of cell adherence and proliferation (Fig. 4E). Two-way ANOVA revealed that the cells on all substrates (TCP, porous and nonporous PGS-M) had significantly higher metabolic rates on day 7 than day 1 ($p < 0.01$, $p < 0.01$, and $p < 0.05$, respectively). A lack of a decrease in metabolic rates suggests the substrates were not cytotoxic. One-way ANOVA showed that metabolic rates were not significantly different between cells on porous and nonporous discs on day 7 of culture.

3.5. Neurite length analysis

NG108-15 cells were cultured on PGS-M hemi-conduits under serum-free conditions to induce neuronal differentiation. At days 4 or 7, cells were labelled via immunocytochemistry for beta-III-tubulin and imaged using confocal microscopy. There was intense background signal on the blue channel due to binding of DAPI to PGS-M hemi-conduits and so this channel was switched off during image processing. Hence, cell nuclei are not visible in these images. Cells successfully differentiated on the surface of the hemi-conduits, as demonstrated by long neurites observed extending from cell bodies (Fig. 5A). Due to the tubular shape of the scaffolds, cells gravitated towards the bottom and as a result grew at a denser concentration than those on the flat TCP control. Two-way

ANOVA with a multiple comparison Tukey's post hoc test showed that the average and maximum neurite lengths of cells on hemi-conduits and TCP were not significantly different from each other.

3.6. Dorsal root ganglion culture

Embryonic chick DRG were isolated and cultured on the NGCs for 14 days. Fig. 6A is a composite of three *z*-stack images showing Schwann cells in green and neurites in red. The DRG in this picture is stuck to the side of the hemi-tube. DAPI was used to stain nuclei of cells, but this could not be visualised due to potential binding of DAPI to or auto-fluorescence of the porous scaffold and subsequent background noise. Schwann cells can be seen along the lumen of the conduits. Fig. 6B shows an image taken on an optical microscope (4 × magnification) of a DRG on TCP control. The maximum distance that Schwann cells migrated from the centre of the DRG is summarised in Fig. 6C.

3.7. Fibroblast infiltration assay

L929 fibroblasts were seeded into 12-well plates containing porous NGCs. Upon seeding, the cells either adhered to the outer or inner walls of the conduits (Fig. 7A, B). Histological images taken on an optical microscope showed that the fibroblasts mostly resided on these surfaces with minimal migration into the scaffolds. The interconnected porous structure can be seen within these images, as well as the portions of nonporous polymer that contribute towards better mechanical strength.

3.8. Fitc-dextran diffusion assay

FITC-dextran was injected into upright porous or nonporous NGCs in water-filled wells. The dextran can be seen fluorescently green in the lumen of the conduits (Fig. 7C, D). The FITC-dextran was no longer visible in porous NGCs after 24 h, indicating that the molecules had diffused through the walls of conduit into the surrounding water. Conversely, the dextran remained as brightly visible in the lumen of the nonporous conduit after 24 h (Fig. 7D), which supports the notion that the result seen in Fig. 7C was due to diffusion and not a weakening fluorescent signal over the 24-hour period.

4. Discussion

Poly(glycerol sebacate)-methacrylate (PGS-M) is a soft and elastomeric material that has been little researched for its use in peripheral nerve regeneration. The two main aims of this study were to i) use novel developments in emulsion templating techniques to make PGS-M nerve guidance conduits (NGCs) with optimal pore size/interconnectivity and mechanical properties and ii) evaluate the *in vitro* and *ex vivo* suitability of these conduits for nerve regeneration.

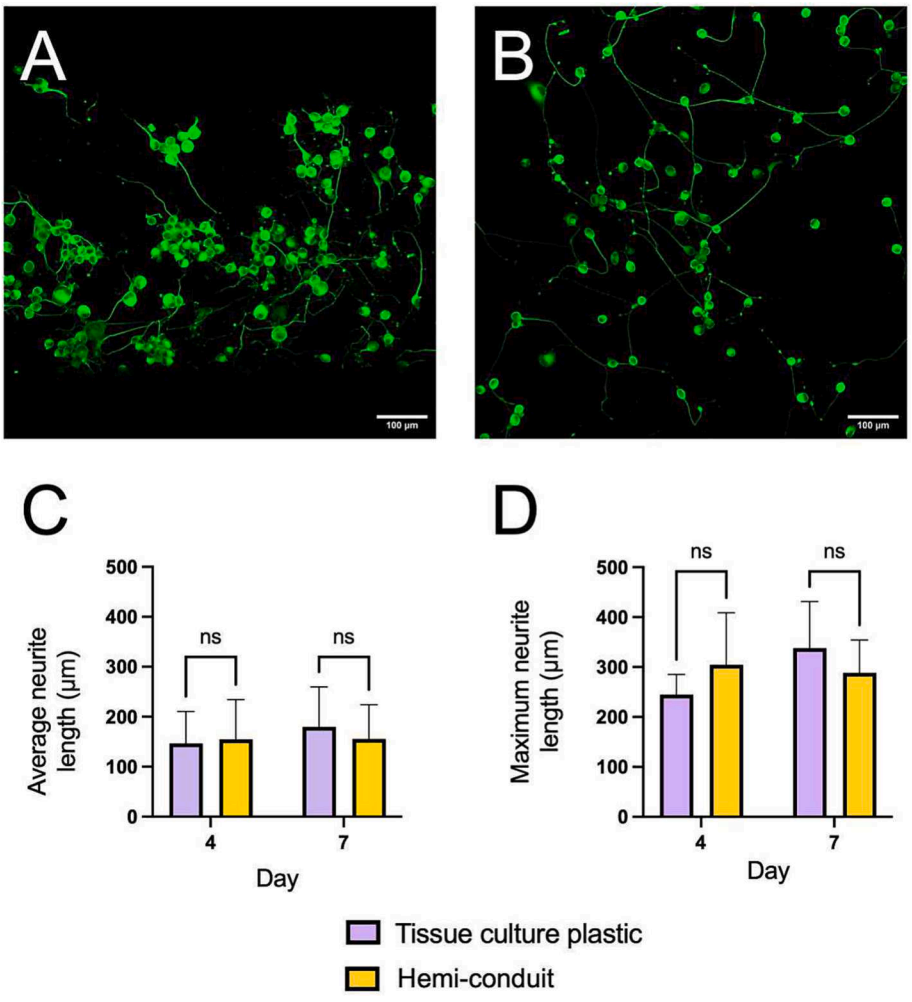

Fig. 5. Neurite length analysis of NG108-15 cells on PGS-M hemi-conduits. A) *Z*-stack projection of NG108-15 cells showing successful neuronal differentiation along the lumen of the hemi-conduits. B) Neuronal differentiation on TCP positive control. C) the average neurite lengths observed on TCP and hemi-conduits. D) the maximum neurite lengths observed on TCP and hemi-conduits. On days 4 and 7, average and maximum neurite lengths were not significantly different between substrates ($p > 0.05$).

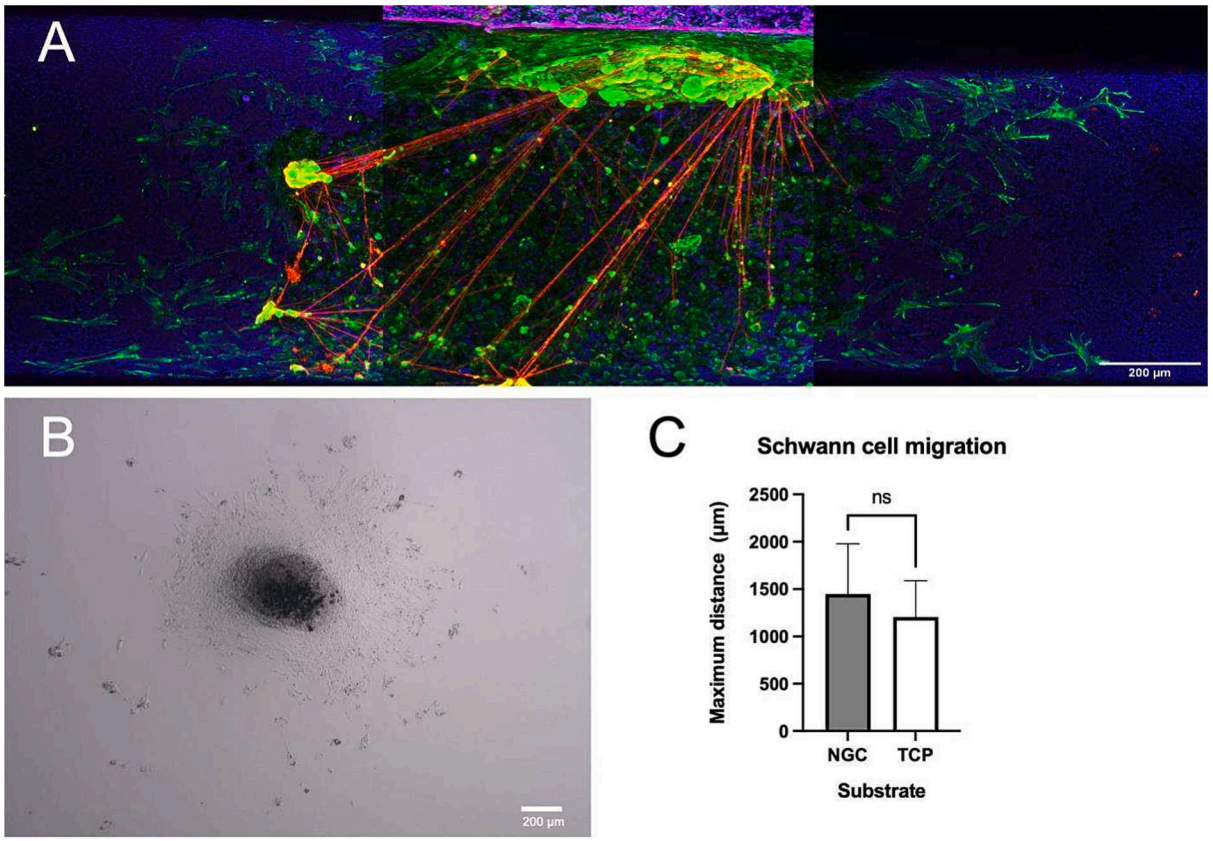

Fig. 6. Embryonic chick dorsal root ganglion (DRG) explant, cultured on porous PGS-M hemi-conduit. A) *Z*-stack projection of a DRG cultured for 14 days on hemi-conduit. Beta-III-tubulin on neurites was labelled red and S100B on Schwann cells labelled green via immunocytochemistry. The conduit itself can be seen as blue due to DAPI staining. B) optical microscope image of DRG on tissue culture plastic (TCP) as control. C) Comparison of the maximum distance Schwann cells migrated away from the DRG on both substrates.

In our study, PGS-M was synthesized via the methacrylation of 80 % of the available hydroxyl groups, resulting in a stiffer material compared to lower percentages of methacrylation [15]. Although a stiffer form of PGS-M was used, polymerised high internal phase emulsions (polyHIPE) scaffolds are rendered weak by the high porosity and when fabricated into nerve guidance conduits (NGCs), would be unable to resist the compressive forces acting upon them *in situ*. This could prove to be problematic as it has been suggested that luminal collapse of NGCs can cause nerve regeneration to fail [25]. In addition, tensile strength is important for NGCs to endure the natural twisting motions of the body. In light of these considerations, an emulsion templating technique was developed in this study by mixing the HIPE with PGS-M polymer in varying quantities prior to UV-curing. This resulted in composite structures with higher tensile and compressive strength than an un-modified polyHIPE. The HIPE + 1G composite had a similar tensile and compressive Young's modulus (0.69 MPa) to that of rat sciatic nerve (0.5 MPa [26]) and rabbit sciatic epineurium and perineurium (0.4 MPa and 3.0 MPa, respectively [27]). This is much closer than other polymers used for nerve regeneration such as PCL or PLA which have bulk elastic moduli of 363.4 MPa [28] and 3.5 GPa [29], respectively.

SEM analysis of the NGCs fabricated with this composite structure revealed how chunks of polymer were dispersed within the porous structure, likely causing the increase in stiffness. The homogenous, interconnected porous structure seen in polyHIPEs was slightly compromised in the polyHIPE/polymer composite. Helium pycnometry allowed for quantification of overall porosity of the structures and a negative correlation was observed between porosity and amount of polymer added. In addition, the mean pore diameter was similar between the HIPE, HIPE + 0.5G and HIPE + 1G groups. Nonetheless there was a much higher standard deviation observed in the composite scaffolds which is attributed to the generation of larger pores in the composites. The pores were much larger, less interconnected and more cavernous in the HIPE + 2G scaffolds.

Although there was a decrease in porosity in the chosen scaffold (HIPE + 1G), the capacity for diffusion remained intact, as demonstrated by the ability of FITC-dextran with a molecular weight of 150 kDa to diffuse through the walls of the conduit into surrounding water. The molecular weight of this type of dextran is significantly larger than the average human protein [30] and molecules such as glucose, indicating that most of the proteins and nutrients involved in wound healing and homeostasis will be able to transfer across the wall. Importantly, the mean pore diameter of these scaffolds was 9.77 ± 7.73 μm, which will likely prove advantageous *in vivo* as a semi-permeable membrane should allow diffusion of nutrients and waste products while obstructing the infiltration of fibroblasts which can lead to scar tissue formation [17,31]. Although some abnormally larger pores can be observed in the cross sections of the conduits, this is unlikely to be problematic as the maximum size of the holes observed on the inner luminal wall was 7.57 μm. This is supported by the results of the fibroblast infiltration assay in our study, in which fibroblasts were unable to migrate through either these holes in the lumen or into the conduit via the outer wall. This is in contrast with a previous study showing that porous PGS-M structures permit fibroblast infiltration over a 7-day period [13]. The surface pores in this study were much larger due to the sucrose porogen leaching technique, which highlights the effectiveness of the smaller pores created in the structures within our study. This indicates that tuning of the surface porosity could yield an effective strategy to obstruct fibroblast infiltration in these devices.

When seeded onto PGS-M discs, the metabolic activity of neuronal-like NG108-15 cells increased over 7 days, indicative of adherence

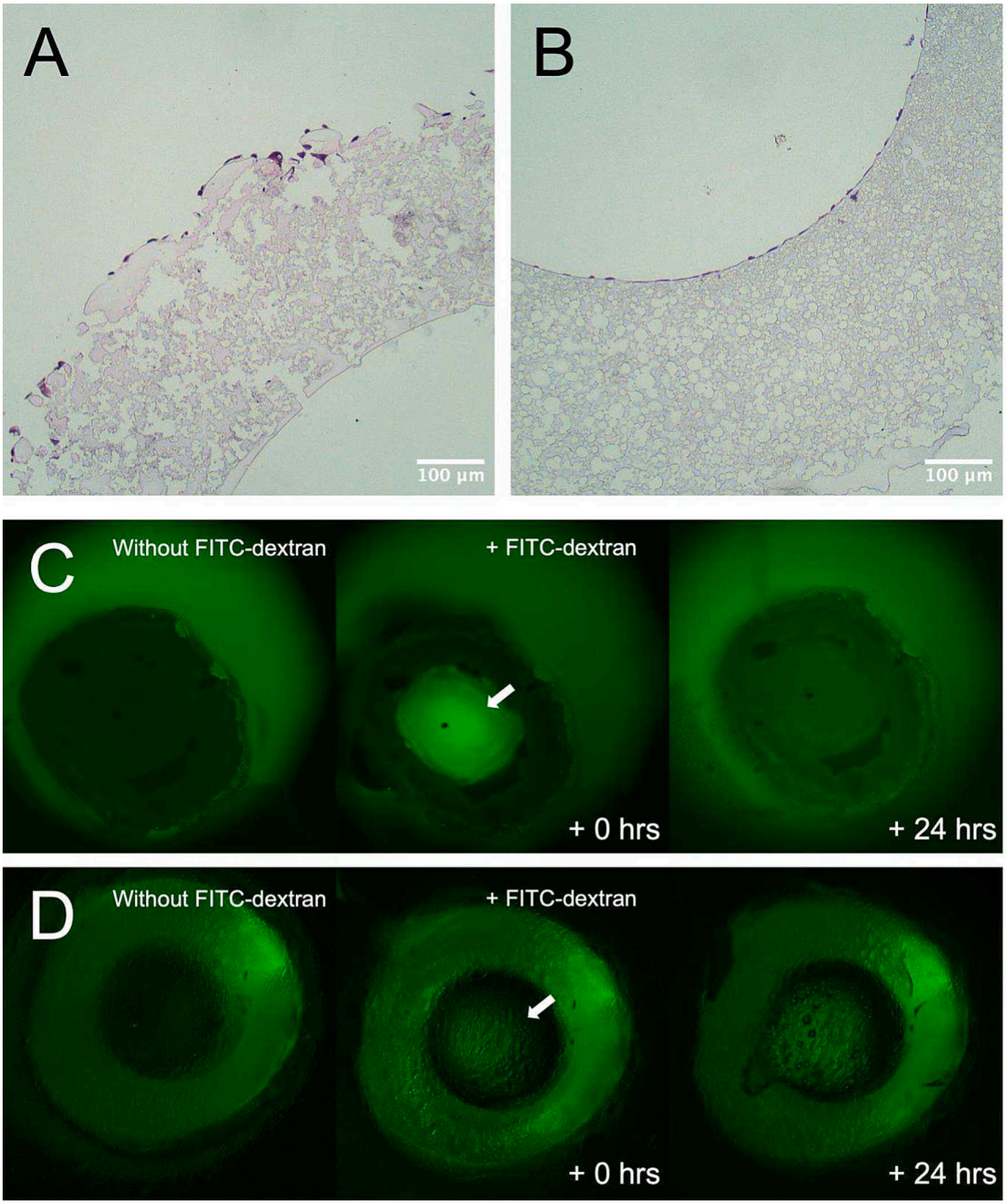

Fig. 7. Semi-permeable nerve guidance conduits (NGCs). L929 fibroblasts were seeded either A) on top of or B) inside the conduits and cultured for 7 days. Histological sections were stained using haematoxylin and eosin. Fibroblasts were observed on either the outer or inner conduit walls, with minimal infiltration into the conduit. C) FITC-conjugated dextran (150 kDa) solution was injected into the lumen of upright NGCs surrounded by water. FITC-dextran had completely diffused through the NGC wall into the surrounding water after 24 h. D) nonporous conduit was used as a control, showing a lack of diffusion after 24 h. White arrows point to the lumen of conduits where the FITC-dextran was injected.

and proliferation. No significant differences were observed between metabolic activity on the porous and nonporous discs, suggesting that the addition of porosity is at the very least not detrimental to cell growth. When seeded onto hemi-conduits and subjected to live/dead staining, an abundance of living cells was observed along the lumen of the conduits after 7 days of culture. Unfortunately, cell viability could not be calculated due to the presence of red fluorescent artefacts on the conduits that had a similar appearance to dead cells when imaged. Nonetheless, the results demonstrate both good cytocompatibility and no cytotoxicity of the PGS-M scaffolds, which are consistent with previous studies [15,14]. When NG108-15 cells underwent neuronal differentiation, neurites were observed extending along the surface of the lumen of hemi-conduits. The average and maximum recorded neurite length was not significantly different between the cells on hemi-conduits and the tissue culture plastic (TCP) positive control. Cell migration was also studied using the embryonic chick DRG, which has been established as a model for nerve regeneration [32–34]. When embryonic chick DRGs were seeded onto hemi-conduits, Schwann cells were observed migrating away from the DRG and along the lumen. This is important as is it believed that Schwann cell migration along the fibrin

matrix that forms in NGCs *in situ* is integral for successful nerve regeneration, releasing neurotrophic factors and guiding the regenerating axons [35]. Furthermore, it could be possible that the axons were following guidance cues secreted by the Schwann cells, as has been seen in previous studies [36]. Our results suggest that porous PGS-M conduits permit the growth of neurites from both the immortalised NG108-15 cell-line and primary neuronal cells. These conduits could be effective in treating PNI, but it is likely that an *in vivo* study of our conduits will be necessary to evaluate their effectiveness further.

5. Conclusion

Nerve guidance conduits (NGCs) are yet to prove as effective as the nerve autograft in the treatment of PNI. Commercially available NGCs have less than desirable mechanical properties and are of a basic design, which limits the success of nerve regeneration. Our study has demonstrated how composite structures comprising nonporous and highly interconnected porous sections can be fabricated via novel developments in emulsion templating techniques. Furthermore, porous NGCs were fabricated using PGS-M, a biocompatible and biodegradable polymer, with similar mechanical properties to that of native nerve tissue. *In vitro,* the conduits were cytocompatible and permissive of neurite outgrowth and Schwann cell migration. Additionally, the conduits were preventative of the infiltration of scar tissue-causing fibroblasts *in vitro* and permissive of small molecule diffusion. These results give an insight as to how semi-permeable PGS-M conduits could be effective for PNI repair. Further work is warranted to evaluate their performance *in vivo*.

Funding

This work was supported by the EPSRC, grant reference: EP/S022201/1; and the Royal Society, grant number: SRF\R1\221053

CRediT authorship contribution statement

Louis D. V. Johnson: Conceptualization, Methodology, Investigation, Validation, Writing – original draft. **Mina Aleemardani:** Writing – review & editing, Supervision. **Simon Atkins:** Supervision, Methodology, Investigation. **Fiona M. Boissonade:** Writing – review & editing, Supervision, Methodology, Funding acquisition, Conceptualization. **Frederik Claeyssens:** Writing – review & editing, Validation, Supervision, Methodology, Investigation, Funding acquisition, Conceptualization.

Declaration of competing interest

The authors declare that they have no known competing financial interests or personal relationships that could have appeared to influence the work reported in this paper.

Data availability

Data will be made available on request.

Acknowledgments

The authors would like to thank the EPSRC funded Centre for Doctoral Training in Advanced Biomedical Materials grant reference EP/S022201/1 for funding this work. FC also thanks the Royal Society for funding of a Royal Society Leverhulme Trust Senior Research Fellowship 2022 (SRF\R1\221053). LJ would like to thank Dr. Sara Memarpour Hobbi, Rachel Furmidge, Boyang Liu, Caitlin Jackson, Dr. Colin Sherborne, Dr. Caroline Taylor and Dr. Matthew Worsley for their help and guidance in the creation of this work. Confocal imaging work was performed at the Wolfson Light Microscopy Facility, using the ZEISS LSM880 AiryScan confocal microscope.

Appendix A. Supplementary data

Supplementary data to this article can be found online at https://doi.org/10.1016/j.matdes.2024.112779.

References

[1] P.N. Mohanna, R.C. Young, M. Wiberg, G. Terenghi, A composite poly-hydroxybutyrate–glial growth factor conduit for long nerve gap repairs, J Anat 203 (6) (2003) 553–565, https://doi.org/10.1046/J.1469-7580.2003.00243.X.
[2] D. R. Peterson, *Biomedical Engineering Fundamentals - Joseph D. Bronzino, Donald R. Peterson - Google Books*, Third. CRC Press, 2006. Accessed: Mar. 08, 2023. [Online]. Available: https://books.google.co.uk/books?hl=en&lr=&id=N4iZBQAAQBAJ&oi=fnd&pg=PP1&ots=t8u6EPhiRO&sig=fMWBA2nVsrYKiCTfDor0Fc5Wfe4&redir_esc=y#v=onepage&q&f=false.
[3] J. Terzis, B. Faibisoff, N. H. Bruce Williams, and C. Montreal, "The Nerve Gap: Suture Under Tension Vs. Graft".
[4] W.Z. Ray, S.E. Mackinnon, Management of nerve gaps: autografts, allografts, nerve transfers, and end-to-side neurorrhaphy, Exp Neurol 223 (1) (2010) 77, https://doi.org/10.1016/J.EXPNEUROL.2009.03.031.
[5] B.E. Fornasari, G. Carta, G. Gambarotta, S. Raimondo, Natural-based biomaterials for peripheral nerve injury repair, Front Bioeng Biotechnol 8 (2020), https://doi.org/10.3389/FBIOE.2020.554257.
[6] F. Xie, F.L. Qing, B. Gu, K. Liu, X.S. Guo, In vitro and in vivo evaluation of a biodegradable chitosan-PLA composite peripheral nerve guide conduit material, Microsurgery 28 (6) (2008) 471–479, https://doi.org/10.1002/MICR.20514.
[7] X. Gu, F. Ding, Y. Yang, J. Liu, Construction of tissue engineered nerve grafts and their application in peripheral nerve regeneration, Prog Neurobiol 93 (2) (2011) 204–230, https://doi.org/10.1016/J.PNEUROBIO.2010.11.002.
[8] J. Braga Silva, B. L. M. Leal, G. A. Magnus, V. de Souza Stanham, R. Mattiello, and C. G. Wolff, "Comparison of nerve conduits and nerve graft in digital nerve regeneration: A systematic review and meta-analysis," *Hand Surg Rehabil*, vol. 40, no. 6, pp. 715–721, Dec. 2021, doi: 10.1016/J.HANSUR.2021.08.006.
[9] Q.Z. Chen, et al., Characterisation of a soft elastomer poly(glycerol sebacate) designed to match the mechanical properties of myocardial tissue, Biomaterials 29 (1) (2008) 47–57, https://doi.org/10.1016/J.BIOMATERIALS.2007.09.010.
[10] R. Rai, et al., Biomimetic poly(glycerol sebacate) (PGS) membranes for cardiac patch application, Mater. Sci. Eng. C 33 (7) (2013) 3677–3687, https://doi.org/10.1016/J.MSEC.2013.04.058.
[11] C.A. Sundback, et al., Behavior of poly(glycerol sebacate) plugs in chronic tympanic membrane perforations, J Biomed Mater Res B Appl Biomater 100B (7) (2012) 1943–1954, https://doi.org/10.1002/JBM.B.32761.
[12] C.D. Pritchard, et al., The use of surface modified poly(glycerol-co-sebacic acid) in retinal transplantation, Biomaterials 31 (8) (2010) 2153–2162, https://doi.org/10.1016/j.biomaterials.2009.11.074.
[13] S. Pashneh-Tala, R. Moorehead, F. Claeyssens, Hybrid manufacturing strategies for tissue engineering scaffolds using methacrylate functionalised poly(glycerol sebacate), J Biomater Appl 34 (8) (2020) 1114–1130, https://doi.org/10.1177/0885328219898385.
[14] I.C. Becerril-Rodriguez, F. Claeyssens, Low methacrylated poly(glycerol sebacate) for soft tissue engineering, Polym Chem 13 (23) (2022) 3513–3528, https://doi.org/10.1039/D2PY00212D.
[15] D. Singh, A.J. Harding, E. Albadawi, F.M. Boissonade, J.W. Haycock, F. Claeyssens, Additive manufactured biodegradable poly(glycerol sebacate methacrylate) nerve guidance conduits, Acta Biomater 78 (2018) 48–63, https://doi.org/10.1016/J.ACTBIO.2018.07.055.
[16] C.L.A.M. Vleggeert-Lankamp, et al., Pores in synthetic nerve conduits are beneficial to regeneration, J Biomed Mater Res A 80A (4) (2007) 965–982, https://doi.org/10.1002/JBM.A.30941.
[17] M. Ezra, J. Bushman, D. Shreiber, M. Schachner, J. Kohn, Porous and nonporous nerve conduits: the effects of a hydrogel luminal filler with and without a neurite-promoting moiety, Tissue Eng Part A 22 (9–10) (2016) 818, https://doi.org/10.1089/TEN.TEA.2015.0354.
[18] S. Atkins, et al., Scarring impedes regeneration at sites of peripheral nerve repair, Neuroreport 17 (12) (2006) 1245–1249, https://doi.org/10.1097/01.WNR.0000230519.39456.EA.
[19] T. Wan *et al.*, "The Porous Structure of Peripheral Nerve Guidance Conduits: Features, Fabrication and Implications for Peripheral Nerve Regeneration," Jul. 2023, doi: 10.20944/PREPRINTS202307.0888.V1.
[20] S. Dikici, B. Aldemir Dikici, S. Macneil, and F. Claeyssens, "Decellularised extracellular matrix decorated PCL PolyHIPE scaffolds for enhanced cellular activity, integration and angiogenesis," *Biomater Sci*, vol. 9, no. 21, pp. 7297–7310, Oct. 2021, doi: 10.1039/D1BM01262B.
[21] S. Caldwell, et al., Degradable emulsion-templated scaffolds for tissue engineering from thiol–ene photopolymerisation, Soft Matter 8 (40) (2012) 10344–10351, https://doi.org/10.1039/C2SM26250A.
[22] B. Aldemir Dikici and F. Claeyssens, "Basic Principles of Emulsion Templating and Its Use as an Emerging Manufacturing Method of Tissue Engineering Scaffolds," *Front Bioeng Biotechnol*, vol. 8, p. 554312, Aug. 2020, doi: 10.3389/FBIOE.2020.00875/BIBTEX.

[23] Y. Wang, G. A. Ameer, B. J. Sheppard, and R. Langer, "A tough biodegradable elastomer," *Nature Biotechnology 2002 20:6*, vol. 20, no. 6, pp. 602–606, 2002, doi: 10.1038/nbt0602-602.
[24] M. Aleemardani, M.Z. Trikić, N.H. Green, F. Claeyssens, Elastomeric, bioadhesive and pH-responsive amphiphilic copolymers based on direct crosslinking of poly (glycerol sebacate)-co-polyethylene glycol, Cite This: Biomater. Sci 10 (2022) 7015, https://doi.org/10.1039/d2bm01335e.
[25] L. Kong, X. Gao, Y. Qian, W. Sun, Z. You, C. Fan, Biomechanical microenvironment in peripheral nerve regeneration: from pathophysiological understanding to tissue engineering development, Theranostics 12 (11) (2022) 4993, https://doi.org/10.7150/THNO.74571.
[26] G.H. Borschel, K.F. Kia, W.M. Kuzon, R.G. Dennis, Mechanical properties of acellular peripheral nerve, J. Surg. Res. 114 (2) (2003) 133–139, https://doi.org/10.1016/S0022-4804(03)00255-5.
[27] S. Koppaka, A. Hess-Dunning, D.J. Tyler, Biomechanical characterization of isolated epineurial and perineurial membranes of rabbit sciatic nerve, J Biomech 136 (2022) 111058, https://doi.org/10.1016/J.JBIOMECH.2022.111058.
[28] S. Eshraghi, S. Das, Mechanical and microstructural properties of polycaprolactone scaffolds with 1-D, 2-D, and 3-D orthogonally oriented porous architectures produced by selective laser sintering, Acta Biomater 6 (7) (2010) 2467, https://doi.org/10.1016/J.ACTBIO.2010.02.002.
[29] S. Farah, D.G. Anderson, R. Langer, Physical and mechanical properties of PLA, and their functions in widespread applications - a comprehensive review, Adv Drug Deliv Rev 107 (2016) 367–392, https://doi.org/10.1016/J.ADDR.2016.06.012.
[30] A. Finka, V. Sood, M. Quadroni, P. D. L. De Los Rios, and P. Goloubinoff, "Quantitative proteomics of heat-treated human cells show an across-the-board mild depletion of housekeeping proteins to massively accumulate few HSPs," *Cell Stress Chaperones*, vol. 20, no. 4, p. 605, Jul. 2015, doi: 10.1007/S12192-015-0583-2.
[31] M.L. Wang, M. Rivlin, J.G. Graham, P.K. Beredjiklian, Peripheral nerve injury, scarring, and recovery, Connect Tissue Res 60 (1) (2019) 3–9, https://doi.org/10.1080/03008207.2018.1489381.
[32] A. Kriebel, M. Rumman, M. Scheld, D. Hodde, G. Brook, J. Mey, Three-dimensional configuration of orientated fibers as guidance structures for cell migration and axonal growth, J Biomed Mater Res B Appl Biomater 102 (2) (Feb. 2014) 356–365, https://doi.org/10.1002/JBM.B.33014.
[33] H.B. Wang, et al., Creation of highly aligned electrospun poly-L-lactic acid fibers for nerve regeneration applications, J Neural Eng 6 (1) (2008) 016001, https://doi.org/10.1088/1741-2560/6/1/016001.
[34] G.P. Williams, G.H. Yam, X.-W. Lee, J.S. Mehta, Validation and quantification of neurotaxis effect in a chick dorsal root ganglion/corneal stromal cell model, Invest Ophthalmol vis Sci 57 (12) (2016) 1920.
[35] J. S. Belkas, M. S. Shoichet, and R. Midha, "Neurological Research A Journal of Progress in Neurosurgery, Neurology and Neuro Sciences Peripheral nerve regeneration through guidance tubes Peripheral nerve regeneration through guidance tubes," 2013, doi: 10.1179/016164104225013798.
[36] D.M. Thompson, H.M. Buettner, Neurite outgrowth is directed by schwann cell alignment in the absence of other guidance cues, Ann Biomed Eng 34 (1) (2006) 161–168, https://doi.org/10.1007/S10439-005-9013-4.